

## MODELLING CROSSHOLE SEISMIC DATA IN STEAM INJECTION PROBLEMS WITH FINITE DIFFERENCES

A. VAFIDIS<sup>1</sup> AND E.R. KANASEWICH<sup>2</sup>

### ABSTRACT

Data from crosshole seismic experiments for monitoring steam injection projects in the Cold Lake area have been compared with realistic computer simulations using finite differences. We perform the simulations on a vector computer with efficient vectorized finite-difference algorithms. Buried line sources of *P*-, *SH*- and *SV*-waves have been implemented employing the technique of Alterman and Karal (1968). These simulations, apart from reconstructing the full wave field, provide insight into the complicated interactions and assist in the interpretation of the real data. They strongly suggest the necessity for two-component acquisition as well as the importance of *S*-waves. These model simulations indicate that seismic experiments, when carefully designed, can play a major role in helping to solve production and recovery problems by determining the spatial distribution of reservoir properties and their changes with time.

### INTRODUCTION

The largest, and potentially the most valuable, of Alberta's subsurface mineral deposits is the crude oil in buried oil sands deposits. Since only 7 percent of these deposits are accessible to surface mining, a large amount of research and many pilot plant studies are being carried out to recover the oil through in-situ methods. Most of these involve the application of heat to reduce the viscosity of bitumen so it may be pumped to the surface. It is always difficult to know the geometry of the heated zone. Drilling is very expensive and not always conclusive as to the properties of the heated zone, since the act of drilling disturbs the fluids and the strata. Crosshole seismic profiling is also expensive at the present time. Before the field procedures are attempted it is useful to conduct computer simulation studies on various methods of carrying out the field work and also to develop methods for the interpretation of complex field data.

One of the main features of a heavy oil is its immobility under formation conditions. Since viscosity decreases drastically with temperature the most widely used recovery technique is cyclic steam injection (Farouq Ali, 1982). This method has certain advantages since the same wells may be used for production and for steam injection. The steam is injected into the well at very high pressures for several weeks and this is followed by a shorter soak period. During this time the rock's temperature increases while the oil becomes mobilized. Then production is started from the same well and the process is repeated many times. One of the very important factors in deciding whether the steam injection must be continued is finding the volume of the steam-heated zone and details of its shape, including preferential propagation paths. The same problem is faced in all thermal recovery techniques (i.e., fire flooding). Seismic experiments (Kanasewich and Vafidis, 1987; Macrides et al., 1988) have proven to be useful tools in imaging steam-heated rocks since they can provide moderate resolution by remote sensing of the anomalous zone.

Several seismic experiments have been conducted by various companies for monitoring steam injection projects in the Cold Lake and Fort McMurray areas of northeastern Alberta. This paper discusses data from these seismic crosshole experiments before and after steam injection. It contains realistic computer simulations using finite differences applied both to the *SH*- and to the *P-SV*-wave equation in two-dimensional heterogeneous media. Vectorized finite-difference algorithms perform efficiently on a vector computer and they increase the applicability of the method. In the next section, we give a short description of the finite-difference method as it is applied to the seismic wave propagation problem. Then, we describe a hole-to-hole experiment conducted in 1982 for monitoring steam injection projects in the Cold Lake area. In simulating this experiment we examine the effects on the seismic response due to changes in the size and shape of the steam-heated zone. Finally, synthetic data are compared with the real data and comments are

Manuscript received by the Editor July 8, 1990; revised manuscript received March 1, 1991.

<sup>1</sup>Formerly, Seismology Laboratory, Department of Physics, University of Alberta, Edmonton, Alberta T6G 3J1; presently, Technical University of Crete, Chania, Greece 73 100

<sup>2</sup>Seismology Laboratory, Department of Physics, University of Alberta, Edmonton, Alberta T6G 3J1

We would like to express our appreciation to the Alberta Oil Sands Technology and Research Authority (AOSTRA) for financial support and to Esso Resources Canada Ltd. for providing the field data. Additional support was provided by the Natural Sciences and Engineering Research Council of Canada (NSERC). The assistance of the supercomputing group at the University of Calgary is deeply appreciated.

included concerning the design of the seismic experiments for monitoring thermal fronts in oil recovery projects.

**SEISMIC WAVE PROPAGATION WITH FINITE DIFFERENCES**

Finite differences can solve numerically either the wave equation or its equivalent system of differential equations. In finite differences both the spatial and time variables are discretized by superimposing a rectangular grid on the model. A difference operator advances in time the response at a particular location employing the present time responses at neighboring locations.

Here, we consider elastic-wave systems that describe *P*- or *S*-waves propagating in two-dimensional heterogeneous media. Two finite-difference schemes form the basis of the algorithms. The first is a novel modified Lax-Wendroff scheme, designed to attain second-order accuracy both in time and space. The second is a one-dimensional MacCormack-type of operator which attains fourth-order accuracy in space and second-order in time when dimensional splitting is applied. Most of the simulations employ the MacCormack scheme, due to its superiority in terms of numerical dispersion effects (Vafidis et al., 1990). All the elastic equations used are written as a first-order hyperbolic system of equations whose coefficients are space-dependent. This heterogeneous approach has the advantage that it is not necessary to introduce boundary conditions at the interfaces.

The *SH*-wave system simulates propagation of one type of body wave only. Its finite-difference solution is very useful in the interpretation since it can describe the propagation of *SH*-waves or acoustic compressional waves without the complexities of conversions. The elastic (*P-SV*) wave system gives a more realistic picture since it describes converted phases. The system in matrix form for the two-dimensional *P-SV*-wave propagation in inhomogeneous media is

$$\partial_t \begin{bmatrix} \dot{u} \\ \dot{w} \\ \sigma_{xx} \\ \sigma_{zz} \\ \sigma_{xz} \end{bmatrix} = \begin{bmatrix} 0 & 0 & \rho & 0 & 0 \\ 0 & 0 & 0 & 0 & \rho \\ \lambda+2\mu & 0 & 0 & 0 & 0 \\ \lambda & 0 & 0 & 0 & 0 \\ 0 & \mu & 0 & 0 & 0 \end{bmatrix} \partial_x \begin{bmatrix} \dot{u} \\ \dot{w} \\ \sigma_{xx} \\ \sigma_{zz} \\ \sigma_{xz} \end{bmatrix} + \begin{bmatrix} 0 & 0 & 0 & 0 & \rho \\ 0 & 0 & 0 & \rho & 0 \\ 0 & \lambda & 0 & 0 & 0 \\ 0 & \lambda+2\mu & 0 & 0 & 0 \\ \mu & 0 & 0 & 0 & 0 \end{bmatrix} \partial_z \begin{bmatrix} \dot{u} \\ \dot{w} \\ \sigma_{xx} \\ \sigma_{zz} \\ \sigma_{xz} \end{bmatrix},$$

or

$$\partial_t U = \mathbf{A} \partial_x U + \mathbf{B} \partial_z U, \tag{1}$$

where  $u(x, z, t)$ ,  $w(x, z, t)$  are the displacements in the  $x$  and  $z$  directions respectively,  $\mu(x, z)$  and  $\lambda(x, z)$  are the Lamé parameters,  $\rho(x, z)$  is the density,  $\partial$  denotes partial derivative,  $\sigma_{xx}$ ,  $\sigma_{zz}$ ,  $\sigma_{xz}$  are the stress components and the dots denote time derivatives.

The *SH* equation may be written as

$$\partial_t \begin{bmatrix} \dot{v} \\ \sigma_{xy} \\ \sigma_{zy} \end{bmatrix} = \begin{bmatrix} 0 & \rho & 0 \\ \mu & 0 & 0 \\ 0 & 0 & 0 \end{bmatrix} \partial_x \begin{bmatrix} \dot{v} \\ \sigma_{xy} \\ \sigma_{zy} \end{bmatrix} + \begin{bmatrix} 0 & 0 & \rho \\ 0 & 0 & 0 \\ \mu & 0 & 0 \end{bmatrix} \partial_z \begin{bmatrix} \dot{v} \\ \sigma_{xy} \\ \sigma_{zy} \end{bmatrix},$$

or

$$\partial_t U = \mathbf{A} \partial_x U + \mathbf{B} \partial_z U. \tag{2}$$

For a liquid, one does not have  $\mu$  but uses  $\lambda$  and obtains an equation similar in general form to the *SH* equation:

$$\partial_t \begin{bmatrix} \dot{u} \\ \dot{w} \\ \tau \end{bmatrix} = \begin{bmatrix} 0 & 0 & \rho \\ 0 & 0 & 0 \\ \lambda & 0 & 0 \end{bmatrix} \partial_x \begin{bmatrix} \dot{u} \\ \dot{w} \\ \tau \end{bmatrix} + \begin{bmatrix} 0 & 0 & 0 \\ 0 & 0 & \rho \\ 0 & \lambda & 0 \end{bmatrix} \partial_z \begin{bmatrix} \dot{u} \\ \dot{w} \\ \tau \end{bmatrix}, \tag{3}$$

where the total stress is given in terms of the normal stress components:

$$\tau = \sigma_{xx} = \sigma_{zz}. \tag{4}$$

The vectorization of finite differences incorporates two modifications:

1. the expression of the finite-difference operators in terms of vector additions and multiplications when the calculations are done on the whole mesh. Utilizing a novel "SuperC" notation applicable to vector supercomputer these operations are easily implemented on a system such as CDC 205 (Abramovici et al., 1987).
2. the vectorized version of matrix by vector multiplication algorithm which consists of a number of vector operations. Here, the matrices are not stored by rows or columns but by diagonals.

For a complete description of the vectorization of finite-difference operators as applied to wave systems the reader is referred to Vafidis (1988) and Vafidis et al. (1990).

One of the key factors in forward modelling is the implementation of the source. Since we are working with three-dimensional problems having an axial symmetry, it is convenient to utilize line sources. Although a point source would be preferred, current limitations on computer memory make it exceedingly expensive to compute a heterogeneous three-dimensional model, particularly when many iterations are necessary. The limitations of a line source are partly mitigated by using the velocity displacement so that the tail which is so prominent on the displacement field is hardly noticed.

The solution of the two-dimensional elastic wave equation in a homogeneous infinitely extended medium with a line source is expressed as a convolution of the impulse response with a source excitation (Aki and Richards, 1980). The convolutional integral is numerically evaluated using Gauss integration. Here a Gaussian function whose frequency response is band-limited with a known peak frequency describes the source excitation.

In *SH*-wave simulation the particle velocity and stresses are calculated by taking partial derivatives of particle displacement with respect to time or space variables. The particle displacement in an isotropic homogeneous medium due to a line source located at  $(x_s, z_s)$  is described by (Aki and Richards, 1980):

$$v(x, z, t) = \frac{H(t - d/c)}{2\pi\rho c^2} \int_0^t \frac{S(t - \tau)}{\sqrt{\tau^2 - \frac{d^2}{c^2}}} d\tau, \quad (5)$$

where  $H(\cdot)$  is a Heaviside step function,  $d$  is the distance from the source location ( $x_s = 0, z_s = 0$ ) to any point on the Alterman and Karal rectangle defining the source region,  $c$  is the phase velocity ( $= 2400$  m/s),  $\rho$  is the density ( $= 2.1$  kg/m<sup>3</sup>) and

$$S(t) = C e^{-\sigma(t-t_1)^2} \quad (6)$$

the source excitation ( $C, \sigma$  and  $t_1$  are constants; the values we use being 1.0,  $0.71 \cdot 10^5$  s<sup>-2</sup>, 0.018 s, respectively).

By taking partial derivatives of equation (5) with respect to  $x, z$  and time we obtain the stress components and the particle velocity. Integrals similar to the one on the right-hand side of equation (5) are present for the stress components and the particle velocity. Notice that the integration interval in (5) increases with time. The source excitation (equation 6) is negligible outside the time window,

$$(t_1 - t_m, t_1 + t_m) \text{ where } t_m = \sqrt{\frac{m}{\sigma}} \ln 10, \quad (7)$$

and in which  $m$  (being equal to 8) is the power of 10 by which the amplitude decays outside the window. Assuming

$$t_m < t_1, \text{ then } t - t_1 + t_m < t.$$

The limits of integration in equation (5) are then replaced by those resulting from the intersection of

$$(t - t_1 - t_m, t - t_1 + t_m) \text{ and } (d/c, t),$$

that is

$$(d/c, t - t_1 + t_m) \text{ for } t < t_1 + t_m + d/c$$

and

$$(t - t_1 - t_m, t - t_1 + t_m) \text{ for } t > t_1 + t_m + d/c.$$

Keeping the integration interval almost constant during Gauss numerical integration, the calculations have uniform level of numerical error. The particle velocity for this line source and its spectrum are shown in Figure 1. The peak frequency in the amplitude response is at 50 Hz, while most of the energy is concentrated at what is called the dominant, 100 Hz in our case, corresponding to the upper frequency at 1/2 of the maximum amplitude.

A similar source excitation has been employed for the  $P$ - $SV$  simulation with either a  $P$ - or an  $S$ -wave line source. For the  $P$ - $SV$  problem in two dimensions, motion is confined to the  $x$  and  $z$  directions only and the displacement may be expressed in terms of potentials as given by (Aki and Richards, 1980):

$$\mathbf{u} = \nabla\phi + \nabla \times [0, \psi, 0]^T = [u, 0, w]^T. \quad (8)$$

For a  $P$ -wave line source the  $SV$  potential ( $\psi$ ) is always zero and the displacement is  $\nabla\phi$ . In this case, convolutional integrals similar to equation (5) exist for the  $\phi$ -potential where the

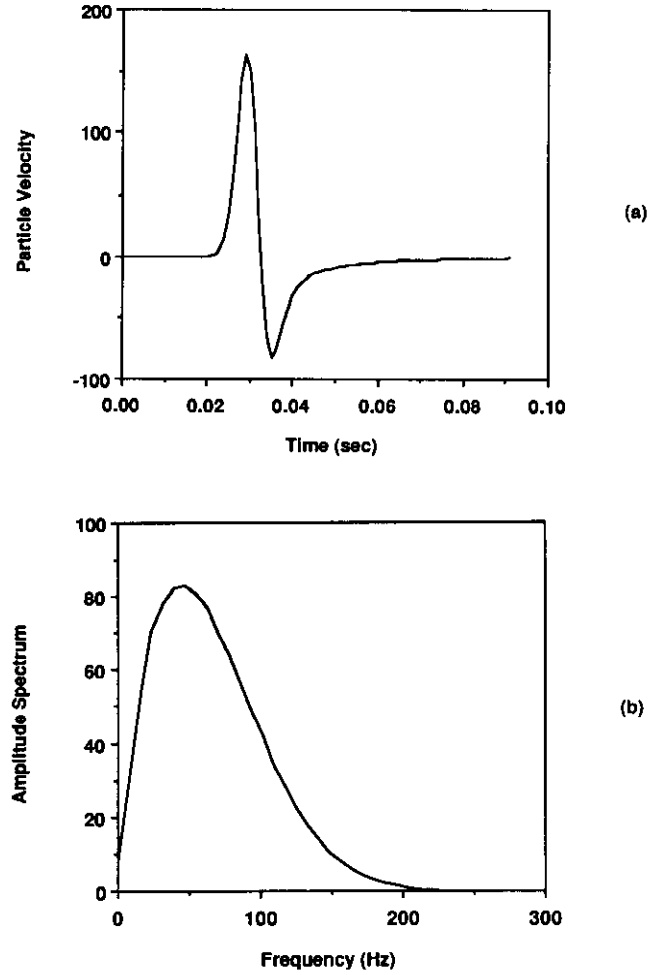


Fig. 1. (a) Particle velocity for a line source with a Gaussian source excitation function ( $\sigma = 0.71 \cdot 10^5$  s<sup>-2</sup>) and time delay 0.018 s; (b) the spectrum of the particle velocity shown in (a).

velocity,  $c$ , is replaced by the compressional velocity. The components of the particle displacement calculated from equation (8) and their first partial derivatives with respect to time and space variables are utilized in the implementation of pure  $P$ -wave line source. A similar expression to equation (5) can be written for the  $\psi$  potential which can be used for a pure  $SV$ -wave line source.

In generating synthetic seismograms for the  $SH$ -wave simulation the following procedure is taken. Firstly, a shear velocity value and a density value are assigned to each grid point. The model parameters, including grid spacing, source and receiver locations, dimensions of the model, etc., must also be specified. It should be noted that any receiver and source geometry can be handled by the program. Secondly, from the stability condition (Vafidis, 1988) and the maximum velocity, the upper limit of the time step is evaluated. Thirdly, the source is inserted in the computational grid through the particle velocity response and the two stress components. The technique of Alterman and Karal (1968) avoids the singularity at the origin and specifies the source on the boundary of a transparent rectangle to avoid problems with internal reverberation of reflections within the

source zone. The difference operator is applied at every grid point in order to advance in time the particle velocity and the stress components. Finally, particle velocity synthetic seismograms are generated at all recording locations in the computational grid by extracting the particle velocity magnitude at those grid points for a sequence of time steps and then plotting these values as time series.

**HOLE-TO-HOLE EXPERIMENT**

The geometry of an initial crosshole experiment at Cold Lake conducted at the end of 1982, shown in Figure 2, consists of one source well and one receiver well separated by 200 m. Ten vertical-component seismometers were employed which recorded at a rate of 1000 samples/second and the shot was located at a depth of 440 m. An explosive source (100 grams of Primacord charge) which contained useable high-frequency signal energy of up to 300 Hz was used, and the records had high signal-to-noise ratio. The heavy oil deposits at Cold Lake lie within the Lower Cretaceous Mannville Group which is subdivided into the McMurray, Clearwater and Grand Rapids Formations (Harrison et al., 1981). From sonic log information the 50-m thick Clearwater Formation has a similar velocity to the Grand Rapids Formation as shown in Figure 3. Steam was injected from a well located half way between the receiver and source wells in the Clearwater. The perforations were at depths

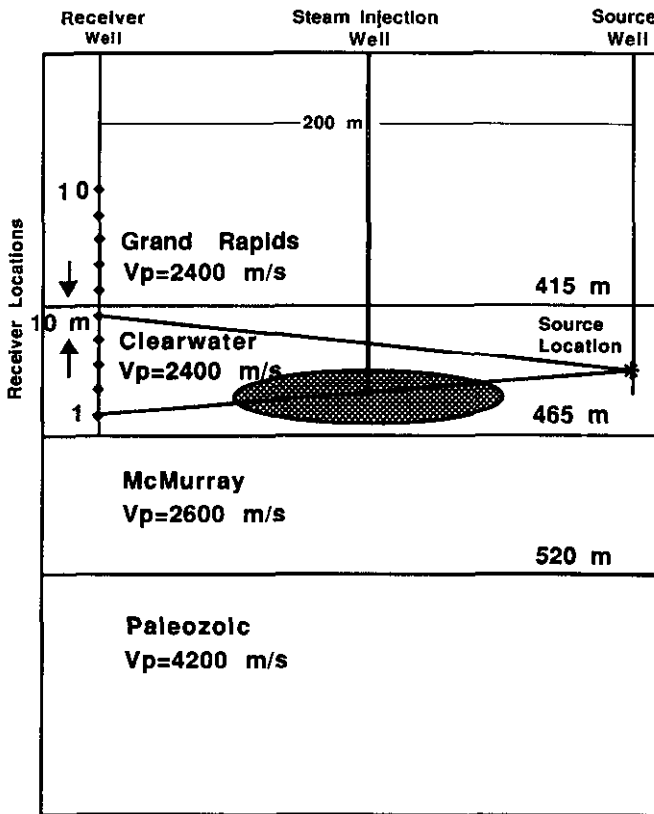


**Fig. 2.** Model geometry for a seismic crosshole experiment. The steam-injection well is located halfway between the source and the receiver wells. The shape of the steam zone is not known and is taken to have an elliptical shape with a *P*-velocity of 1800 m/s. The receiver separation is 10 m.

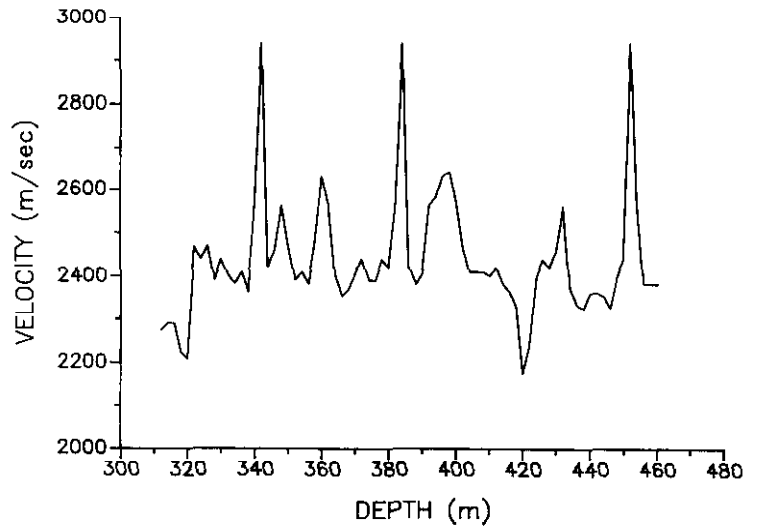


**Fig. 3.** Sonic log at the receiver well after sampling at 2-m sampling interval. The boundary between the Grand Rapids and the Clearwater Formations occurs at 415 m. The high-velocity stringers are due to zones of calcite and from other logs in the region these are seldom continuous for more than several tens of metres.

between 442 and 450 m. The depths to the interfaces were derived from well-log data (Kanasewich, 1983).

The experiment was conducted twice, the first time before steam injection and the second after injecting steam at a pressure of 10 MPa for 48 days. The first 250 ms of the before and after steam injection experiments are shown in Figure 4 where the seismic signals are rectified in such a way as to allow plotting the *before* records (blue colour) entirely above the zero amplitude baseline and the *after* records (red colour) entirely below it. The original positive parts of the signals are shaded with the appropriate colour. This display is called BARS (Before/After Rectified Seismic) plots. The amplitudes of the arrivals from the two experiments show significant changes on receivers 2 to 5 and are lower in the after-steam traces. Notice the very low amplitudes of the *S*-waves after injection. Also, definite time delays of up to 2 ms in the *P*-wave arrivals are observed in the after-steam experiment due to propagation through the low-velocity steam zone. Reflections from layers below the Clearwater are difficult to identify in the records. Vafidis et al. (1987) and Macrides et al. (1988) studied extensively this data set and, based on evidence from theoretical and experimental studies, Nur et al. (1980) and Tosaya et al. (1984) modelled it with rays and a *P*-wave velocity drop of 20 percent within the steam zone. Under this condition, delays of less than 2 ms are associated with a steam zone 29 m wide for *P*-wave velocity 2.4 km/s. The *S*-wave arrivals (traces 1 and 2 on the right-hand quarter of the BARS plot in Figure 4) have delays which are considerably larger (up to 10 ms), indicating substantial changes to the *S*-wave velocity which is not predicted from laboratory experiments. Neither the before nor the after *S*-wave velocities are known in this case.

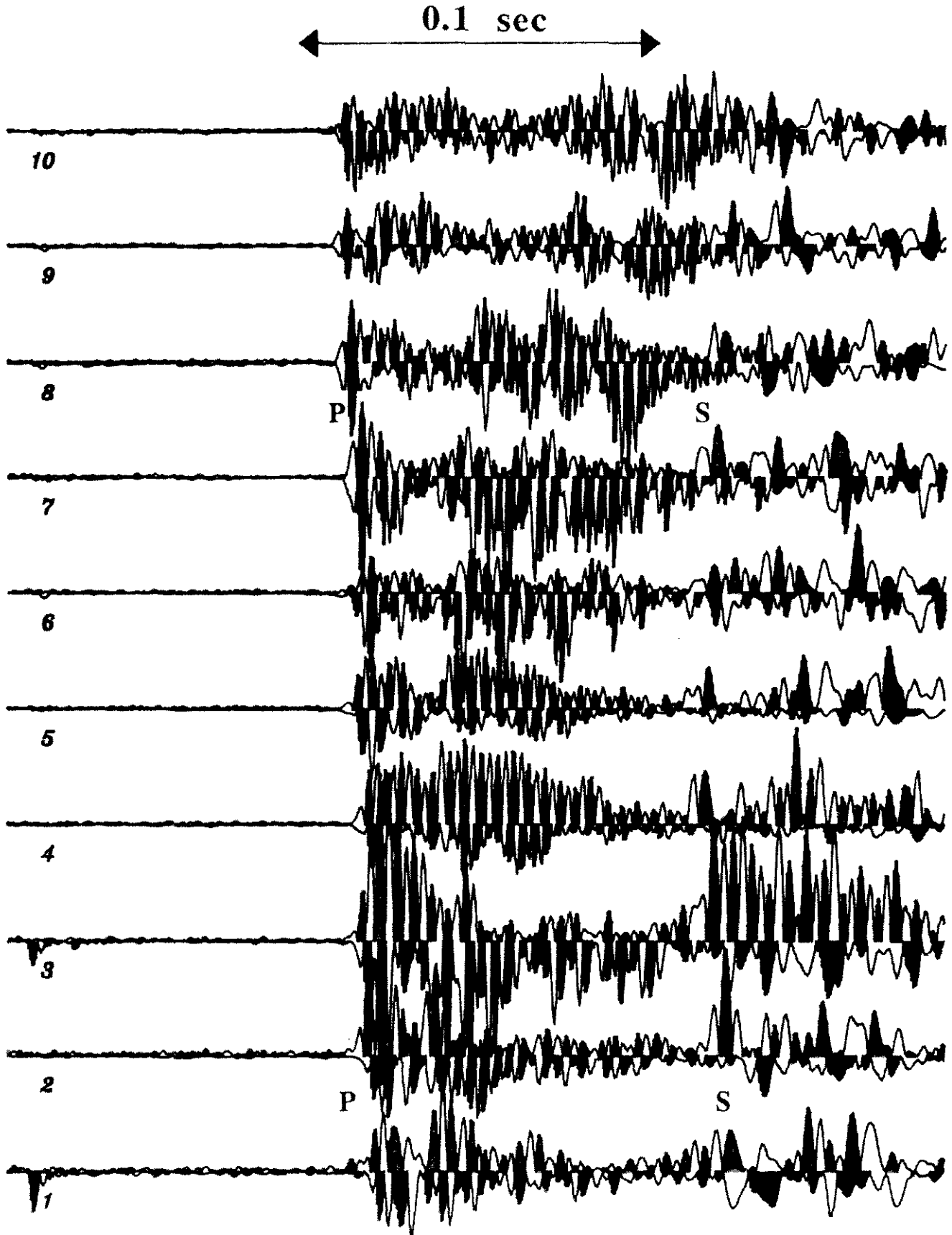


Fig. 4. BARS plots for a steam injection experiment. The seismic signals are rectified in such a way as to allow plotting the *before* records (blue colour) entirely above the zero amplitude baseline and the *after* records (red colour) entirely below it. The original positive portions of the signals are shaded by the colour. The original negative parts are unshaded.

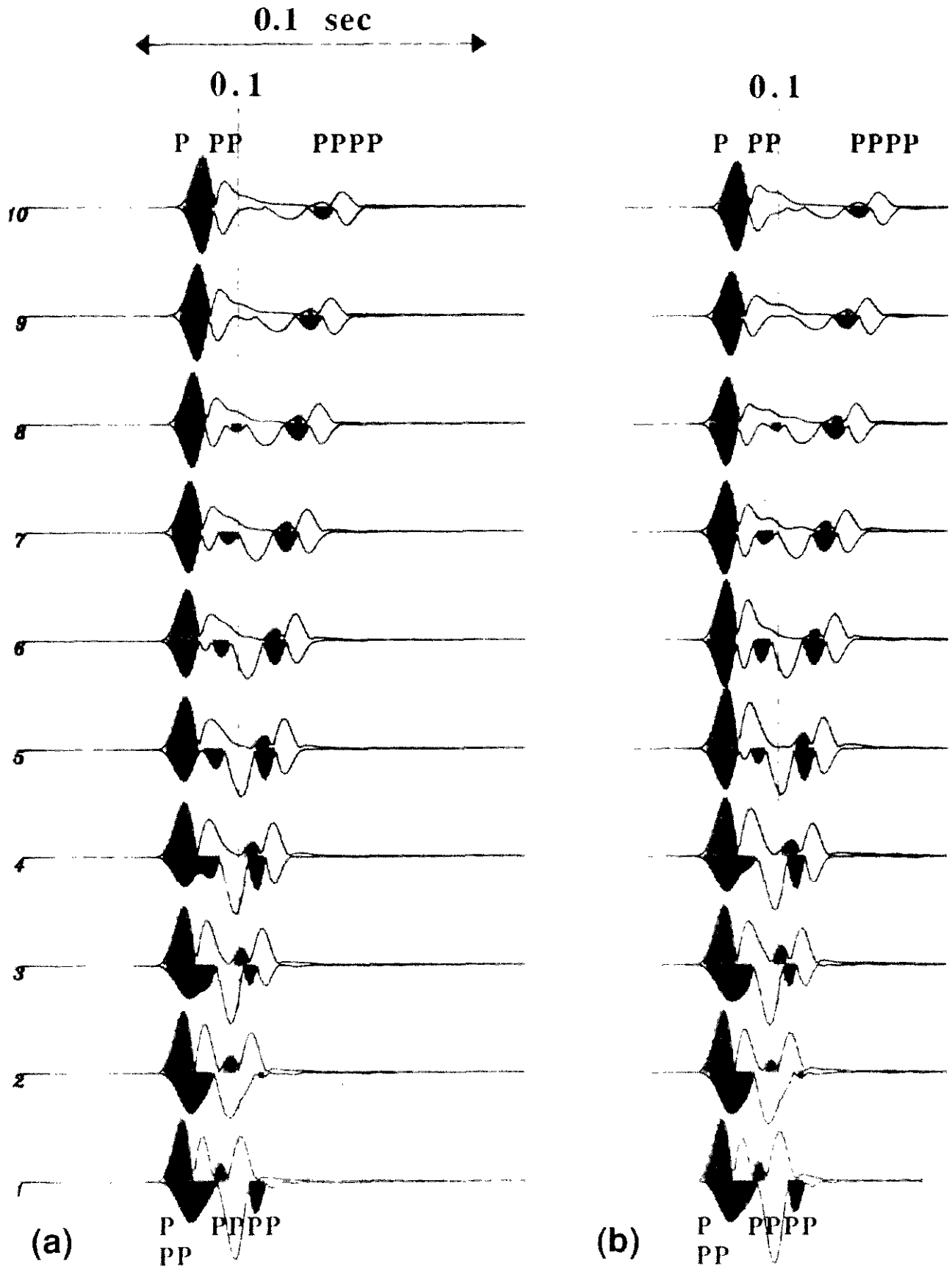


Fig. 5. (a) BARS plots for an acoustic wave computer simulation of the 1982 crosshole experiment; (b) the same as in Figure 4a but velocity varies vertically according to the sonic log.

**Table 1.** Numerical parameters — crosshole experiment.

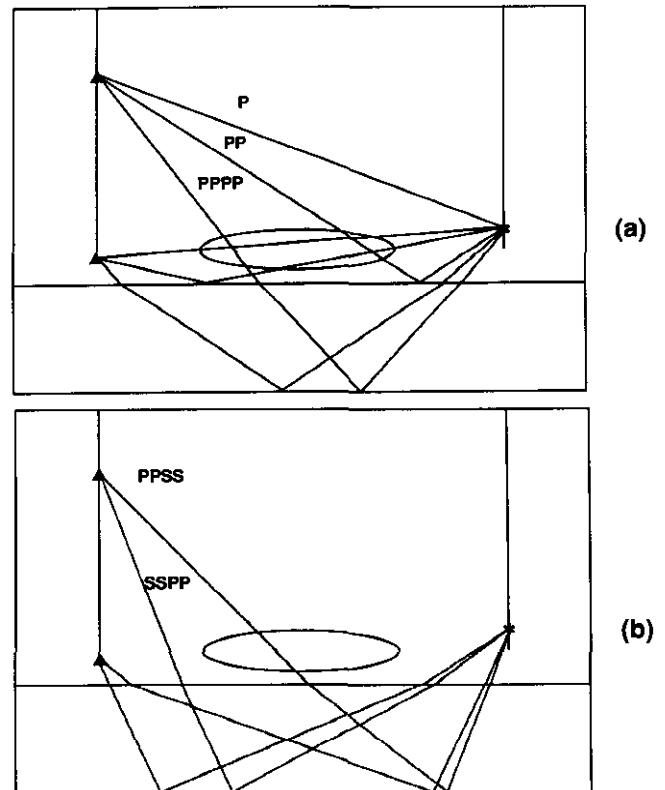
Source:	$t_f = 18$ ms;	Minimum velocity: 1800 m/s
$\sigma$	$0.71 \cdot 10^5 \text{ s}^{-2}$	
(wavelength = 15 m)		
Receiver separation:		10 m
Grid spacing:		2 m
Time step:		0.1 ms
Semixis of the ellipse:		
Major:		24 m
Minor:		5 m

### SIMULATION WITH ACOUSTIC SYNTHETIC F.D. ALGORITHM

Computer seismic-wave simulations were carried out for the crosshole experiment employing a high-frequency (100 Hz) line source whose excitation function is Gaussian-shaped. The numerical parameters are shown in Table 1. The *SH*-wave equation is similar to the acoustic wave equation (if you use *P*-wave instead of *S*-wave velocities) and may be used to model compressional velocities. Figure 5a shows the first 120 ms of the seismic rectified records in an acoustic simulation before and after steam injection for the model shown in Figure 2, while Figure 6a illustrates selected rays for the same geometry. The traces before steam injection show the direct arrivals as well as reflections from the McMurray and Paleozoic. The reflections (PP) from the McMurray interface are very weak due to small velocity contrast. The reflections from the Paleozoic (PPPP) can provide additional information about the low-velocity region. After steam injection, strong events that arrive at 100 ms are present in addition to the events seen in the before steam injection experiment. Also, delays of 2 to 3 ms in the direct arrivals are measured in the after steam injection experiment for rays passing through the low-velocity steam zone.

The results from the acoustic computer simulation of the 1982 experiment, shown in Figure 5a, give a simplistic but very useful view of the effects of the steam zone. As a next step, a more detailed model based on sonic log information is employed in the simulation. The velocities, after redigitization at 2-m sampling interval, are displayed in Figure 3. The exceptionally high velocities at depths 340 m and 380 m may correspond to calcite stringers which are present in the Grand Rapids Formation. They are very thin and discontinuous layers with velocities of up to 5000 m/s. In the sonic log, resolution problems do not permit the evaluation of the correct velocity and thickness of the calcite stringers. Usually, the stringers are displayed with lower velocity and larger thickness.

In this simulation, the dominant frequency is 100 Hz and for an average velocity,  $v = 2400$  m/s, the dominant wavelength is 24 m. The resolution of the synthetic data is one-quarter to one-eighth of the wavelength, that is 6 to 3 m. In the real data, the dominant frequency is around 240 Hz and the corresponding wavelength 10 m. Calcite stringers have thicknesses of less than 2 m. The resolution of the real data is 2.5 m, which is still greater


**Fig. 6.** Ray diagrams for the 1982 crosshole experiment: (a) *P* arrivals before steam injection and (b) converted arrivals before steam injection.

than the thickness of the stringers. The results from this simulation (Figure 5b) look quite similar to the previous ones. So the small variations in the sonic velocity to the formation do not affect the propagation as drastically as the presence of the steam zone. Our synthetic seismogram experiments indicate that one would require a seismic source spectrum with dominant energy above 300 Hz before one could distinguish the effect of these layers on the seismic records.

### SIMULATION WITH *P*-*SV* SYNTHETIC F.D. ALGORITHM

Next, a *P*-*SV* computer simulation was carried out in order to include converted phases. The particle velocity components in the vertical (*x*) and horizontal (*z*) directions are displayed for the before and after steam injection experiments (Figures 7 and 8). A high-frequency *P*-wave line source, with dominant frequency 100 Hz is employed to excite the system. Since the explosive source in a cylindrical hole generates both *P*- and *S*-waves, one includes by linear superposition an *SV* line source whose frequency content is up to 60 Hz. The response is about one-half that generated on the field data, but it was difficult to simulate this with the required smaller grid on the Cyber 205 computer because of memory limitations and excessive paging. The responses from the *P* and *SV* line source simulations are combined and the vertical- and horizontal-component sections are displayed in Figures 7 and 8.

Clear direct *P* arrivals are present whose energy is recorded mostly on the horizontal-component receiver (Figure 8). Delays

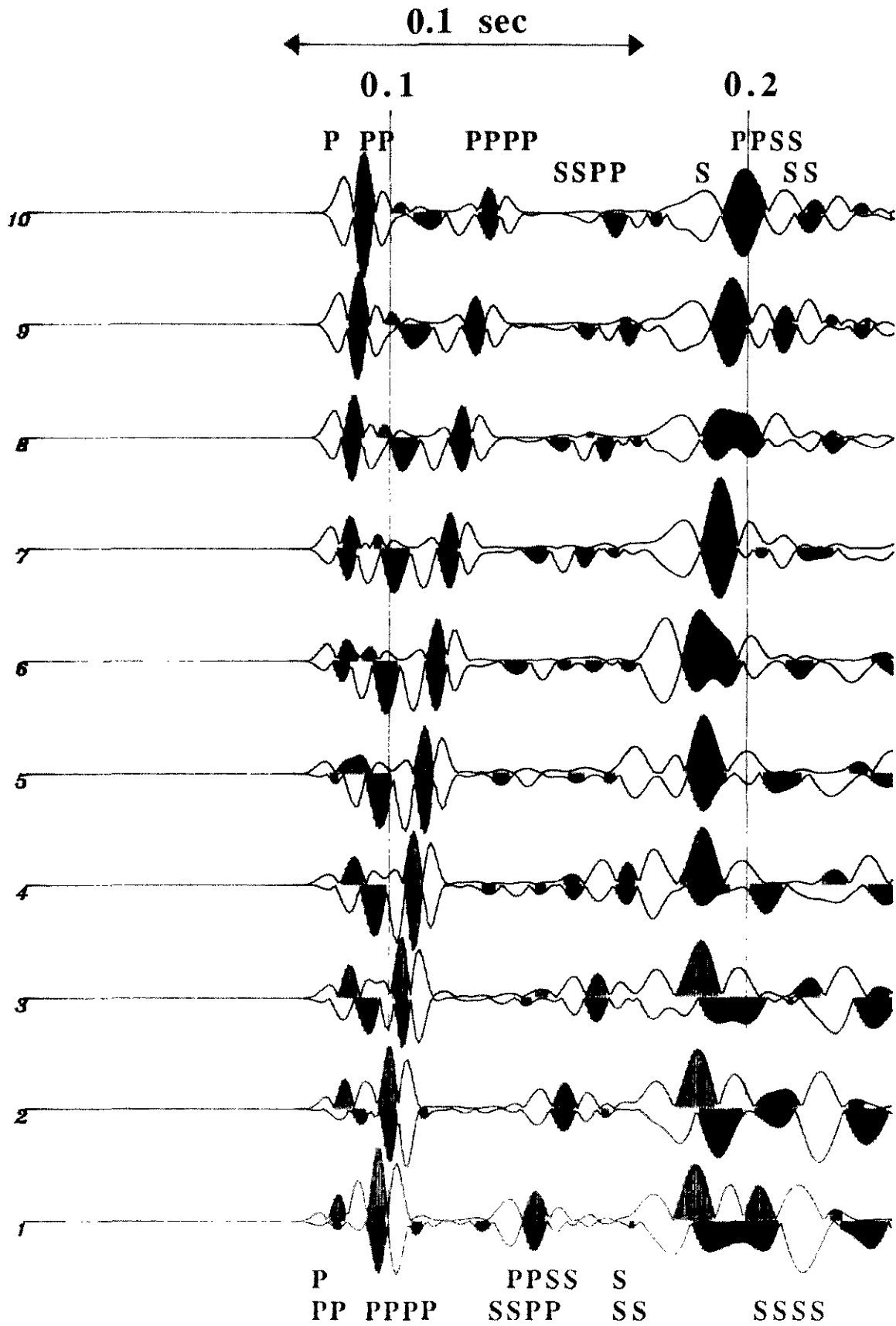


Fig. 7. BARS plots for a *P-SV* computer simulation of the crosshole experiment obtained by summing the *P*- and the *SV*-wave line source results. This shows the vertical component of particle velocity.



of up to 2 ms are measured in the direct  $P$  arrivals after steam injection for the first five receivers, in agreement with the real experiment. For the reflected upgoing  $P$ -waves most of the energy is recorded on the vertical component (Figure 7). Reflections from the interfaces below the Clearwater may be clearly observed in the before traces. Reflections from the top and the bottom of the steam zone are also observed in the after traces (3 to 8) at approximately 100 ms. The reflected and direct  $P$  events described above look similar to the ones simulated from the acoustic ( $SH$ ) program using  $P$ -wave velocities. Apart from those events,  $SV$ -converted phases (PPSS) reflected from the top of the Paleozoic formation are present at around 180 ms and show no delays after steam injection. Given suitable source and receiver locations, these phases could be useful for resolving the extent of the steam-heated zone in the region between the injector and the receiver wells.

Direct  $S$ -waves are recorded on the vertical component which are delayed in the after steam injection experiment by 5 to 10 ms for receivers 1 to 3. Those delays are similar to the ones observed in the real experiment and may give useful information concerning the shape and the size of the heated zone. In the synthetic sections, the direct  $S$ -wave can be completely resolved and this helps to identify it in the real sections. The delays on the direct  $S$ -wave arrivals can be explained by the increase of the Poisson ratio from 0.36 outside the steam-heated zone to 0.4 inside. This is an indication that the zone is dominated by steam condensate rather than steam. Notice the reflections (SSSS) from the Paleozoic at around 200 ms for receivers 1 to 6 mostly on the vertical component. Finally, the converted phases (SSPP) are present at earlier times (120 ms) on both components, since the angle of emergence is about  $45^\circ$ , and have relatively small amplitudes.

The real data in Figure 4 shows similar delays on both the  $P$ - and  $S$ -wave phases for raypaths that pass through the anomalous steam zone. The  $S$ -wave pattern shows similar phase and amplitude changes apart from the difference in source frequencies. The response from the simulation as it is recorded on the vertical-component geophones is comparable to the outcome from the real data. In the computer seismic-wave simulation above, the size of the steam zone is larger (48 m wide) than that proposed by Macrides et al. (1988) which produces the same delays in the  $P$ - and  $S$ -wave direct arrivals after steam injection. Macrides et al. (1988) based their calculations on simple straight ray theory. Simple ray theory is adequate for most purposes in applied seismology but it does not give a complete physical description of seismic phenomena. In this experiment, the rays diverge from the low-velocity steam zone (Phadke and Kanasewich, 1990) and straight ray theory fails to predict this effect. In wave theory this effect is taken into account, so observed delays correspond to larger low-velocity zones. Finite differences give a more complete picture of the experiment where, apart from the delays, information about the amplitudes is preserved. Unfortunately, there are no borehole measurements which will give the actual size of the anomalous region.

We have obtained a better model using forward modelling of the real experiment. This should provide a better understanding

of the complex processes by identifying direct, reflected or converted events. Apart from identifying the various phases we can make very useful observations on how their amplitudes are affected by the presence of the heated zone. The simplistic shape of the steam zone (ellipse) seems to be a good first approximation which introduces most of the events that are present in the real experiment. A band of events not present in the simulations recorded between 150 to 180 ms may be due to high-velocity discontinuous stringers which are present in the Clearwater Formation but their exact disposition cannot be determined from the limited number of sonic logs. Another possibility is that those thin (2 m) calcite stringers are continuous but they prograde so that they appear at different depths on different wells. The shape of the steam zone is also more complex than the simple elliptical shape we have specified. It is worth noting that those simulations, apart from reconstructing the full wave field, gave us insight on which rays are converted and so aided in the interpretation of the real data. Finally, this study strongly suggests the necessity for two-component acquisition as well as the importance of  $S$ -waves.

## CONCLUSIONS

Seismic methods can play a role in helping to solve production and recovery problems by determining the spatial distribution of reservoir properties and their changes with time. Since large velocity changes occur upon heating in porous media with heavy hydrocarbons, the seismic measurements might be used to track temporal and spatial changes in physical conditions associated with the thermal recovery techniques. Computer simulations can tell us how to extract information about the direction of propagation and details of the shape, rate of movement and spatial heterogeneity of the steam front. The variety of the seismic effects discussed above and the sensitivity of density and velocity to reservoir parameters clearly indicate the future direction of reservoir seismology. It appears possible to describe reservoirs in more detail and to monitor their modification, particularly if high-frequency sources can be used together with high-resolution seismic recording techniques. These could include use of repetitive small explosives, buried geophones and systems that record at 1/2 or 1/4 ms sampling intervals.

## REFERENCES

- Abramovici, F., Vafidis, A. and Kanasewich, E.R., 1987, Supercomputer programs for solving elastic wave propagation problems in two-dimensions: Proc. Supercomputing Symposium '87, Calgary, Canada.
- Aki, K. and Richards, P., 1980, Quantitative seismology, theory and methods, Vol. I: W.H. Freeman & Co.
- Alterman, Z. and Karal, F.C., 1968, Propagation of elastic waves in layered media by finite-difference methods: Bull. Seis. Soc. Am. **58**, 367-398.
- Daley, P.F. and Hron, F., 1979,  $SH$  waves in layered transversely isotropic media — an asymptotic expansion approach: Bull. Seis. Soc. Am. **69**, 689-711.
- Farouq Ali, S.M., 1982, Elements of heavy oil recovery: Univ. of Alberta Press.

- Harrison, D.B., Glaister, R.P. and Nelson, H.W., 1981, Reservoir description of the Clearwater oil sand, Cold Lake, Alberta, Canada, *in* The future of heavy crude and tar sands: McGraw-Hill Inc., 264-279.
- Kanasewich, E.R., 1983, Cold Lake seismicity project: report No. 3: Dept. of Physics, Univ. of Alberta.
- \_\_\_\_\_ and Vafidis A., 1987, Simulation of seismic wave propagation in oil sands projects on the supercomputer: *Super-C Newsletter* 3, 4, 7-10.
- Macrides, C., Kanasewich, E.R. and Bharatha, S., 1988, Cross-borehole seismic imaging in steam injection projects: *Geophysics* 53, 65-75.
- Nur, A., Walls, J.D., Winkler, K. and De Vilbiss, J., 1980, Effects of fluid saturation on waves in porous rock and relations to hydraulic permeability: *J. Soc. Petr. Eng.* 20, 450-458.
- Phadke, S. and Kanasewich, E.R., 1990, Ray and spectral modelling of low velocity steam zones: *Geophys. Res. Lett.*, submitted.
- Tosaya, C.A., Nur, A.M. and Da Prat, G., 1984, Monitoring of thermal EOR fronts by seismic methods: western energy frontiers: *Proc. Soc. Petr. Eng.* 54, 179-186.
- Vafidis, A., 1988, Supercomputer finite-difference methods for seismic wave propagation: Ph.D. thesis, Univ. of Alberta.
- \_\_\_\_\_, Abramovici, F. and Kanasewich, E.R., 1987, Supercomputer finite-difference algorithms for use in seismic tomography as applied to oil sands projects: 57th Ann. Internat. Mtg. and Exposition, Soc. Expl. Geophys., New Orleans, Expanded Abstracts.
- \_\_\_\_\_, \_\_\_\_\_ and \_\_\_\_\_, 1991, Elastic wave propagation using fully vectorized high order finite-difference algorithms: *Geophysics*, in press.